Journal of Power Sources 242 (2013) 824–831

Contents lists available at SciVerse ScienceDirect

Journal of Power Sources

journal homepage: www.elsevier.com/locate/jpowsour

Effect of tar fractions from coal gasification on nickel–yttria stabilized zirconia and nickel–gadolinium doped ceria solid oxide fuel cell anode materials

E. Lorente [a], C. Berrueco [b,1], M. Millan [b,*], N.P. Brandon [a]

[a] Department of Earth Science and Engineering, Imperial College London, London SW7 2AZ, UK
[b] Department of Chemical Engineering, Imperial College London, London SW7 2AZ, UK

HIGHLIGHTS

- Influence of gasification tar fractions on anode carbon formation was studied.
- Lighter tar fractions were predominantly responsible for carbon formation.
- Ni/CGO presented less carbon deposition than Ni/YSZ regardless the tar fraction.

ARTICLE INFO

Article history:
Received 7 March 2013
Received in revised form
15 May 2013
Accepted 29 May 2013
Available online 10 June 2013

Keywords:
Gasification tar
Tar distillation fractions
SOFC anodes
Carbon formation

ABSTRACT

The allowable tar content in gasification syngas is one of the key questions for the exploitation of the full potential of fuel cell concepts with integrated gasification systems. A better understanding of the interaction between tars and the SOFC anodes which leads to carbon formation and deposition is needed in order to design systems where the extent of gas cleaning operations is minimized. Model tar compounds (toluene, benzene, naphthalene) have been used in experimental studies to represent those arising from biomass/coal gasification. However, the use of toluene as a model tar overestimates the negative impact of a real gasification tar on SOFC anode degradation associated with carbon formation.

In the present work, the effect of a gasification tar and its distillation fractions on two commercially available fuel cell anodes, Ni/YSZ (yttria stabilized zirconia) and Ni/CGO (gadolinium doped ceria), is reported. A higher impact of the lighter tar fractions was observed, in terms of more carbon formation on the anodes, in comparison with the whole tar sample. The characterization of the recovered tars after contact with the anode materials revealed a shift towards a heavier molecular weight distribution, reinforcing the view that these fractions have reacted on the anode.

1. Introduction

Solid oxide fuel cells (SOFCs) coupled with coal/biomass gasifiers offer the potential of highly efficient combined heat and power production [1]. The theoretical performance expected from integrated gasifier and SOFC systems has been investigated by several authors [2–8]. Electrical efficiencies above 50% and overall system efficiencies exceeding 80% have been predicted for those systems with simultaneous heat and material integration between the SOFC and gasification unit [2,6]. A higher efficiency translates in reduced emissions and extended fuel reserves.

The gaseous product resulting from gasification is an energy rich mixture, and its composition depends on a number of variables, including the reactor type, gasification agent, feedstock, and operating conditions of the gasification process. It consists to a major extent of hydrogen and carbon monoxide, the balance being carbon dioxide, methane and other hydrocarbon species, water vapour and nitrogen (in case of air as the gasification agent). The gas also contains diverse impurities such as particulates, ammonia, hydrogen sulphide, hydrogen chloride, alkali metals, metals, and tars.

The presence of impurities is one of the main concerns for any application of the syngas. Due to the different amount and types of contaminants present in gasification syngas, the detrimental effects of a specific impurity are often unclear. Depending on the nature of the downstream application, it may be necessary to remove any or all of these impurities before the syngas can be used. Thus, gas

* Corresponding author. Tel.: +44 (0)2075941633; fax: +44 (0)2075945638.
E-mail address: marcos.millan@imperial.ac.uk (M. Millan).
[1] Current address: Bioenergy and Biofuels Area, Catalonia Institute for Energy Research, IREC, 43007 Tarragona, Spain.

0378-7753/$ – see front matter © 2013 Elsevier B.V. All rights reserved.
http://dx.doi.org/10.1016/j.jpowsour.2013.05.158

cleaning systems are usually designed to meet the specific requirements of the end-use application.

The feasibility of operating a SOFC directly on gasification syngas has been demonstrated experimentally [9–11]. However, these experimental studies report the use of a gas pre-treatment unit to remove a large extent of the impurities before the gas is supplied to the fuel cell. A number of critical challenges related to the extent of gas cleaning required for its use in SOFC remain to be addressed for the development of this technology. A thorough knowledge of the interactions between the various species in coal/biomass-derived syngas and SOFC anodes is essential to successfully design and optimize this process.

The syngas purity required by SOFCs is not known in detail, and there are discrepancies on the reported acceptable levels for the concentration of impurities, even for similar types of fuel cells [12]. These discrepancies are, for example, due to electrode material and/or microstructure differences, or diverse operating conditions. In some cases, the presence of certain impurities causes immediate performance degradation. More often, the deterioration occurs over a long period depending on the permissible exposure to the specific harmful species. Different contaminants in the fuel stream can lead to different types of performance degradation depending on the chemical nature of the impurity, concentration level and mechanism of poisoning. Several studies, both theoretical and experimental, have reported the effect of potential contaminants present in gasification-derived syngas on the performance of SOFCs, mostly focussing on hydrogen sulphide and to a minor extent on ammonia and hydrogen chloride [13–16].

However, when discussing the impact of contaminants in syngas derived from biomass and/or coal gasification, tar has been recognized to pose the greatest problem [17–20]. Tar is a complex mixture of organic condensable compounds formed by aromatics and polycyclic aromatic hydrocarbons (PAH). The amount and composition of the tar present in syngas largely depends on the type of feedstock as well as the operating conditions and gasifying agent [21–24]. It is well known that tar can be decomposed catalytically with nickel [25], which is one of the main constituents of anode materials, and this may favour the development of carbon deposition on the anode, leading to a reduction in the electrical efficiency and durability of the fuel cell. The carbon formation depends on the operating conditions of the cell, e.g., the steam to fuel ratio, temperature, current density, etc., as well as on the anode material and its characteristics (composition and morphology) [26,27]. Other factors are tar content and quality, and overall gas composition.

Tar concentration in the syngas can be minimized by designing and operating the gasifier maximizing cracking in the char bed [28]. Tars are also removed in downstream gas cleaning, through condensation by decreasing the gas temperature or by catalytic tar cracking. However, these operations add to the complexity of the process, resulting in efficiency and economic penalties. Establishing the SOFCs tolerance limits to tar will in turn specify the requirements for appropriate gas cleaning systems and tar abatement strategies, and will avoid their over-design, with its negative impact on the economic viability of the process.

Thermodynamic equilibrium analyses have been performed with the aim of predicting carbon formation on Ni-containing anodes due to tars present in the fuel from a gasifier [29]. The impact of various parameters like current density, steam and temperature have been studied in order to determine a suitable range of operating conditions at which carbon deposition can be minimized. This type of analysis can be used as an initial design tool to provide an estimate of the level of tar removal required from cleanup technologies. However, experiments have demonstrated that carbon deposits can form even under conditions where a carbon solid phase is not thermodynamically favoured [30,31].

Experimental studies are needed for a better understanding of the interaction between tars and the SOFC anodes which leads to carbon formation and deposition. Such information is applicable to mitigating deactivation, and to developing more tolerant and stable anode materials. Fuel cell behaviour has been investigated by feeding the system with pure aromatic compounds, such as toluene [32], benzene [33], or naphthalene [34,35] as model tars. However, a previous study showed that the use of toluene as a model tar overestimates the negative impact of a real gasification tar on SOFC anode degradation associated with carbon formation [36].

The present work aims to investigate the effect of tar fractions with different boiling point ranges derived from a real gasification tar on two commercially available fuel cell anodes, Ni/YSZ (yttria stabilized zirconia) and Ni/CGO (gadolinium doped ceria), in order to establish the relative contribution of each fraction to carbon formation and cell deactivation.

2. Experimental

2.1. Materials

2.1.1. Anode powders

The anode catalysts under study were NiO/YSZ (yttria stabilized zirconia) and NiO/CGO (gadolinium doped ceria), sourced from Fuel Cell Materials. The powders contain 66 wt% and 60 wt% of NiO, for NiO/YSZ and NiO/CGO, and the surface areas are 6.21 $m^2\ g^{-1}$ and 5.6 $m^2\ g^{-1}$, respectively.

Both materials were calcined at 1300 °C in air for 1 h and then sieved to a particle size of 125–250 μm, before the reaction tests.

2.1.2. Tar samples

A tar sample from a coal gasifier and its fractions was used in this study. The isolation of the tar fractions was performed by distillation of the whole tar sample using a microdistillation apparatus (Sigma Aldrich), at atmospheric pressure. Two lower boiling fractions, herein named Fraction 1 and Fraction 2, were collected. Fraction 1 had a boiling point up to 150 °C and Fraction 2 boiled between 150 °C and 250 °C. The distillation residue (Fraction 3), with a boiling point above 250 °C, was very viscous. Table 1 presents the weight contribution of the three individual fractions to the weight of the whole tar.

2.2. Reaction system and procedure for carbon deposition tests

A fixed bed flow reactor under atmospheric pressure was used for the study of carbon deposition behaviour of tar and tar fractions over the nickel based anode materials. A schematic diagram of the experimental set-up is shown in Fig. 1.

40 mg of anode material was placed as a powder on a piece of quartz wool in the 6 mm OD quartz tube reactor. The reactor was heated to a typical SOFC operating temperature of 765 °C at a rate of 10 °C min^{-1} in a dry nitrogen atmosphere. In order to reduce the

Table 1
Weight percentage and density of tar fractions obtained by distillation of a coal tar sample.

Fraction	Temperature range	wt%	Density (g mL^{-1})
1	<150 °C	22.6	0.82
2	150 °C–250 °C	39.5	1.00
3	>250 °C	37.9	n.a.

n.a. not analysed.

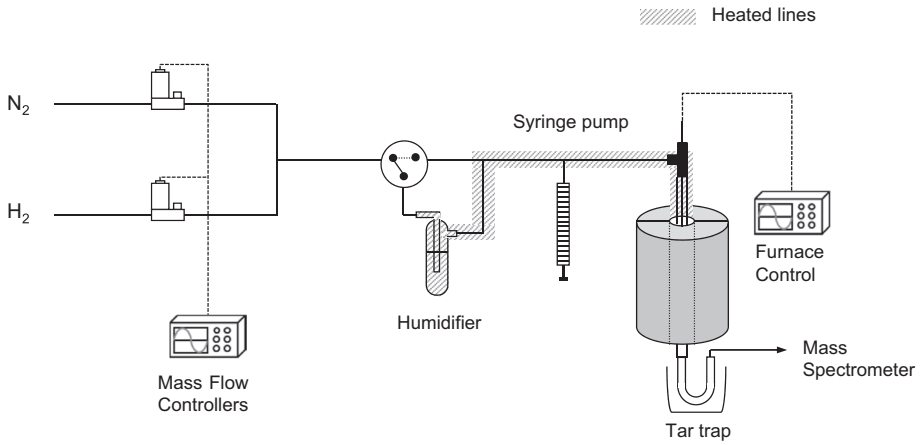

Fig. 1. Schematic diagram of the reaction system.

catalysts to Ni, a 2.5% H_2O in H_2/N_2 mixture was employed, with increasing concentrations of H_2, from 5% to 25%, over a reduction period of 90 min. The H_2 concentration was then changed to the experimental operating conditions of 15%, keeping the steam content at 2.5% (N_2 balance). Steam was produced in a humidifier by bubbling the gaseous mixture through water at 21 °C. The total flow rate during heating, reduction and reaction was fixed at 100 NmL min^{-1}.

Tar was injected employing a syringe pump (KD Scientific) at a rate of 100 μL h^{-1}, producing a tar concentration of 13.7–16.7 g Nm^{-3} (depending on the tar density). The feed line was heated and insulated and the temperature was controlled to be slightly above the boiling point of each tar sample, to allow for vaporization of the tar species into the gas phase, and subsequent mixing with the incoming gas.

The discharge from the reactor passed through a tar trap connected at the reactor outlet. The trap consisted of a stainless steel U-tube, packed with stainless steel mesh and immersed in an ice-water bath, to ensure efficient condensation of the tar vapour.

Downstream, an online mass spectrometer (Thermo Fisher Prolab) was employed for gas analysis. The main gaseous products detected during the carbon deposition experiments were carbon monoxide, carbon dioxide and methane. The concentration of these species (not shown) was used to evaluate the overall carbon balance closure, which was better than 96% for all the experiments.

Anode catalyst samples were exposed to tar for 1 h. After 1 h, the tar flow was stopped and the reactor was cooled to room temperature in a 15% H_2/N_2 dry stream in order to avoid Ni and carbon oxidation. At the experimental conditions of the present study (low hydrogen concentration and temperatures below 765 °C), it is not expected that significant amounts of carbon are removed from the surface of the anode materials in the cool-down period [37–39]. Tar was recovered by washing the tar trap and the bottom part of the reactor with a mixture of chloroform and methanol in the ratio 4:1 (in volume). The resulting solution was then dried in a recirculating oven at 35 °C for 2 h and kept for further analysis. The tar recovery procedure was carried out with fresh tar samples, and it was confirmed that the volatile loss during drying was negligible.

The amount of deposited carbon (W_{carbon}) on the anode materials was measured by weight difference of the samples before and after reaction ($W_{initial}$ and W_{final}, respectively), taking into account the weight loss due to the reduction (assumed complete) of NiO to Ni ($\Delta W_{reduction}$), according to Eq. (1).

$$W_{carbon} = W_{final} - (W_{initial} - \Delta W_{reduction}) \quad (1)$$

2.3. Characterization techniques

2.3.1. Ultimate analysis

The carbon, hydrogen, sulphur and nitrogen contents of the tar samples were determined with a LECO TruSpec-CHN/S analyzer. The oxygen content was obtained by difference. The analyses were performed with 0.1 g of sample. The results were quoted as the mean of values from four determinations. In all cases, the experimental error was <0.5% of the absolute value.

2.3.2. Temperature programmed oxidation (TPO)

TPO experiments of the reacted anode samples were carried out to confirm the amount and determine the properties of the carbon deposited on the catalysts. About 15 mg of the reacted anode materials was heated in a fixed bed flow reactor at 10 °C min^{-1} up to a final temperature of 800 °C. Oxidation of the carbon was driven by flowing 80 NmL min^{-1} of a 2% O_2 balance argon gas, while a mass spectrometer (Thermo Fisher Prolab) was used to monitor the CO_2 concentration of the effluent gas stream.

2.3.3. Size exclusion chromatography (SEC)

A 300 mm long, 7.5 mm i.d. polystyrene/polydivinylbenzene-packed Mixed-D column with 5 μm particles has been used (Polymer Laboratories, Church Stretton, UK). The column was operated at 80 °C and a flow rate of 0.5 mL min^{-1}. N-methyl-2-pyrrolydinone (NMP) was used as the mobile phase. Detection was carried out using a Knauer Smartline diode array UV-absorbance detector. As NMP is opaque at 254 nm, detection of standard compounds and samples was performed at 270 and 300 nm respectively, where NMP is partially transparent. Estimates of molecular masses were calculated from a mass calibration based on the elution times of polystyrene standards (PS) and PAH standards. The calibration and methodology have been reported elsewhere [40,41].

2.3.4. Ultraviolet fluorescence spectroscopy (UV-F)

A Perkin–Elmer LS55 luminescence spectrometer equipped with a quartz cell of 1 cm path length was used to obtain emission, excitation and synchronous spectra of the tar samples, using NMP as solvent. The spectrometer was set with a slit width of 5 nm, to scan at 500 nm min^{-1}. Only synchronous spectra, which were acquired at a constant wavelength difference of 20 nm, are shown. All spectra were measured in dilute solutions, as this avoids self absorption effects. The full methodology has been reported elsewhere [42].

2.3.5. Gas chromatography (GC)

GC analyses of the tar samples were performed on a Perkin–Elmer Clarus 500 chromatograph, with a Flame Ionization Detector and a high-temperature capillary column (HT5 phase, 25 m length, 0.032 mm i.d., 0.1 μm film thickness, from SGE). Helium was used as carrier gas at a flow rate of 1 mL min^{-1}.

The column oven temperature was programmed from 40 °C (held for 1 min) to 380 °C, at 10 °C min^{-1} and held for 10 min. The programmed-temperature injector was operated in split mode (ratio 10:1) and its temperature was ramped from 80 °C to 350 °C at 100 °C min^{-1} and held for 5 min.

3. Results and discussion

3.1. Characterization of fresh tar

The whole tar sample and its distillation fractions were characterized by an array of techniques: ultimate analysis, SEC, UV-F and GC.

3.1.1. Ultimate analysis

The ultimate analysis data of the samples are given in Table 2. It shows that the coal tar sample had a relatively low nitrogen content (~1.3 wt%) and an average sulphur content: ~0.6 wt%. The results indicate significant changes in hydrogen and oxygen (decreased), carbon and nitrogen (both increased) contents with the distillation fraction boiling point. Sulphur content was similar for all fractions.

Oxygen functionalities appear to be concentrated in the lighter fractions, which also are less aromatic (lower C/H ratio). On the other hand, the heavier fractions contain nitrogen functionalities with higher carbon content, indicating a higher aromaticity and lower aliphatic content.

3.1.2. Size exclusion chromatography

SEC was used to estimate the molecular weight distribution of the tar samples. The chromatograms, represented in Fig. 2, are plotted as signal (area normalized) vs. elution time. The SEC chromatogram of the whole tar sample presents a small early-eluting peak (at around 10–11 min). This peak corresponds to material unable to penetrate the porosity of the column packing, and referred to as "excluded" from the column porosity. The second eluting band (between 17 and 25 min) represents the material able to penetrate the porosity of the column packing. The lift-off of this band occurs at around 17 min, which corresponds to a mass of about 6500 u according to the PS calibration. A maximum intensity peak and a second peak can be observed at 350 u and 200 u, respectively.

The SEC analyses of Fractions 1 and 2 resulted in similar chromatograms, without excluded peak and lift-off at masses around 1000 u and 1300 u, for Fraction 1 and Fraction 2, respectively. Two peaks can be clearly distinguished for both samples; the maximum is located at 120 u (Fraction 1) and 140 u (Fraction 2) and the second peak at 315 u (Fraction 1) and 330 u (Fraction 2).

Table 2
Ultimate analysis of tar samples.

Sample	Ultimate analysis (wt%)					C/H[b]	C/O[c]
	C	H	N	S	O[a]		
Whole tar	83.6	7.80	1.27	0.56	6.8	0.9	16.4
Fraction 1	81.4	9.76	0.43	0.51	7.9	0.7	13.7
Fraction 2	83.0	9.14	1.14	0.56	6.2	0.8	18.0
Fraction 3	84.8	7.03	1.71	0.49	5.9	1.0	19.0

[a] By difference.
[b] Carbon/hydrogen atomic ratio.
[c] Carbon/oxygen atomic ratio.

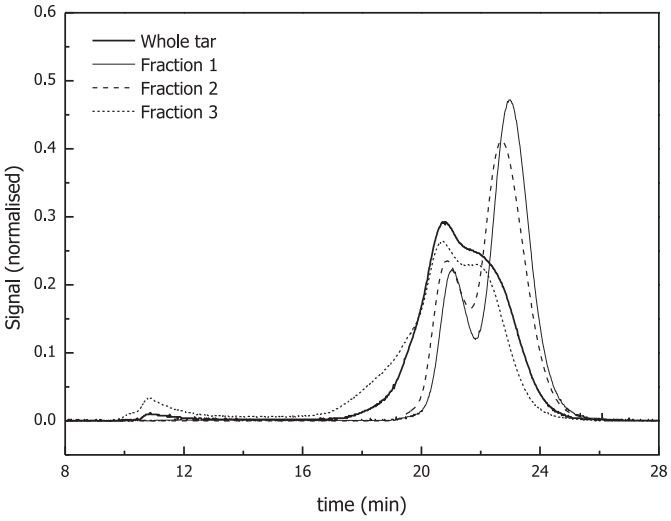

Fig. 2. SEC chromatograms of the fresh tar samples.

The molecular weight distribution of Fraction 3 closely resembles that of the whole tar sample. The chromatogram presents an excluded peak, the lift-off of the retained band is located at around 9500 u and the maximum intensity peak and second peak are at 370 u and 200 u, respectively.

3.1.3. UV-F spectroscopy

UV-F analyses of the whole tar and tar fractions were performed to gain information about differences in the aromatic chromophore size of the molecules present in the samples. The synchronous UV-fluorescence spectra (height normalized) are shown in Fig. 3. The spectra of the whole tar sample and Fraction 3 do not show significant differences in the range of chromophores detected (similar to results obtained by SEC), showing that the spectra are dominated by the larger PAH groups. On the other hand, a shift in the spectra of Fraction 1 and Fraction 2 towards shorter wavelengths can be observed, which is related to the presence of smaller aromatic chromophore sizes in these samples.

3.1.4. Gas chromatography

The tar fractions were examined by GC and the resulting chromatograms are plotted in Fig. 4. As expected, there was a

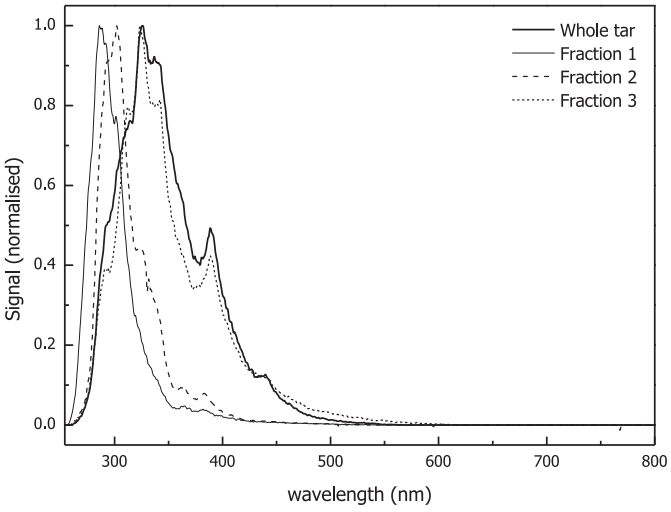

Fig. 3. UV-F synchronous spectra of the fresh tar samples.

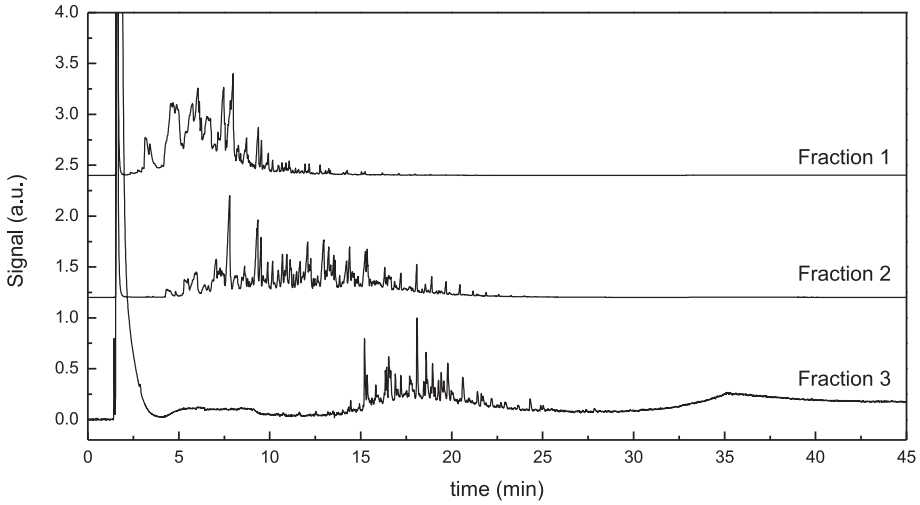

Fig. 4. GC chromatograms of the fresh tar samples.

correlation between the boiling point range of each fraction and its GC elution times, with some degree of overlapping between fractions due to the effect of chemical structure on GC elution. The peak distribution ranged from 3 to 14 min for Fraction 1, from 5 to 22 min for Fraction 2 and from 15 to 26 min for Fraction 3. Fraction 1 clearly extended towards shorter retention times, which indicates the presence of lighter species as compared to the other tar fractions.

In summary, the characterization of the tar distillation fractions by ultimate analysis, SEC, UV-F and GC show that, although there is some overlap among them, the tar fractions present different properties and essentially differ from the whole tar sample. As the fraction boiling point increases, the fractions contain progressively higher molecular weight species with larger polyaromatic groups. The impact of using the lighter tar fractions (Fraction 1 and Fraction 2) on SOFC will be analysed and compared with the effect of the whole tar.

3.2. Comparison of the effect of tar fractions on carbon deposition

Experiments were performed in order to investigate the behaviour of a real tar sample and its distillation fractions (Fraction 1 and Fraction 2), during their interaction with SOFC anode materials, Ni/YSZ (yttria stabilized zirconia) and Ni/CGO (gadolinium doped ceria). The tar distillation residue (Fraction 3) was not used in the carbon deposition tests, since the material was very viscous and could not be injected in the gas stream. The degree of carbon formation on the anode materials was examined using the experimental set-up described in the Experimental section. The anode materials were exposed to tar (13.7–16.7 g Nm^{-3}) in a gas stream composed of 15% H_2 and 2.5% H_2O, balance N_2, at 765 °C for 1 h.

Analyses were carried out on (i) carbon deposits on the anode catalysts and (ii) tar collected downstream from the anode catalyst bed after reaction.

3.2.1. Carbon deposits

The amounts of carbon deposited on the catalyst materials in experiments performed with the coal tar and its fractions were quantitatively analysed. The measured values are represented in Fig. 5, as a percentage of total carbon content of each tar sample. In order to determine the total carbon content of tars in a volume of sample used for each experiment (100 μL), the values of density measured (given in Table 1) and wt% of C (from elemental analysis) were used. The values of total carbon in the 100 μL tar samples were found to decrease in the order: whole tar (84.5 mg), Fraction 2 (82.9 mg) and Fraction 1 (66.7 mg). The significantly lower value obtained for the latter is due to its lower density.

It can be observed in Fig. 5 that Ni/CGO presents a better performance (less carbon formation) than Ni/YSZ at the experimental conditions of this study. This result was expected due to the ability of ceria to resist carbon deposition [43].

Regarding the comparison among tar and tar fractions, it can be seen that for both anode materials the degree of carbon formation due to the tar distillation fractions was considerably higher than the amount of carbon formed over the catalyst exposed to the whole tar sample. On the other hand, the amounts of carbon deposits obtained with Fraction 1 and Fraction 2 were similar. However, as the same tar volumetric flowrates were used in both cases, experiments with Fraction 1 were carried out at higher steam-to-carbon ratio (S/C = 1.21 vs. S/C = 0.97 for Fraction 2) and the anodes were exposed to a lower total amount of carbon during the run, as a result of its lower density. When these slight differences in operating conditions are factored in, it seems that Fraction 1 has a higher propensity to carbon formation on the anode material than Fraction 2. This trend of lighter fractions leading to more intense

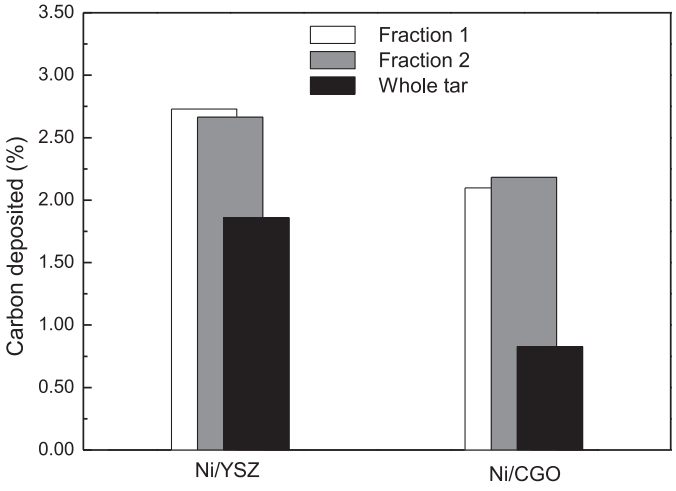

Fig. 5. Amount of carbon deposited (as a percentage of total carbon content in tar samples) over Ni/YSZ and Ni/CGO, exposed to 2.5% humidified steam, 15% H_2, and 14–17 g Nm^{-3} tar for 1 h at 765 °C.

carbon formation is in agreement with previous findings [36], which showed that the use of a light tar analogue (toluene) resulted in more carbon deposition than experiments performed with a real gasification tar (containing heavier hydrocarbons). Comparison between the extent of carbon deposition in the experiments using toluene reported in Ref. [36] and the tar fractions used in this study reinforce this view, as toluene resulted in significantly larger carbon formation than either fraction.

To gain information on the nature of the carbon formed on the anode catalysts, the samples were further tested by temperature programmed oxidation analysis, as shown in Fig. 6A and B, for the series of tests with Ni/YSZ and Ni/CGO, respectively. The TPO analyses revealed that the carbon deposited on Ni/YSZ and Ni/CGO resulting from exposition to Fraction 2 can be removed at a lower temperature compared to the carbon formed after exposure to the whole tar sample. On the other hand, the TPO curves of the materials following contact with Fraction 1 presented the main peak at a slightly higher temperature than the peak of the whole tar sample. This fact is related with more intense polymerization of the tars during the coke formation process and a higher level of graphitization of this coke.

It has to be noted that the reactivity of aromatic hydrocarbons to form carbon is related to a combination of chemical and physical factors. The chemistry of carbonization is complex, involving a myriad of chemical reactions, many occurring simultaneously.

It is well known that chemical structure controls the degree of graphitization of organic materials [44]. However the relation between the starting structure and the final carbon properties is not always obvious. Substitution on the aromatic ring can alter the course of graphitization. In particular the oxygen functionalities may evolve towards disordered carbon or graphite like structures if present as oxygenated aromatics or oxygen-containing compounds, respectively.

3.2.2. Characterization of tars following contact with the anode

In order to investigate changes in the properties of the tar fractions after contact with the anode materials, the tar samples collected after each carbon deposition experiment were characterized by SEC, UV-F and GC.

SEC chromatograms of the condensable tar samples recovered after the carbon deposition tests are represented in Fig. 7A and B for experiments with Fraction 1 and Fraction 2, respectively. For comparison, the analyses of the fresh tar samples are also included. The following changes can be noticed in the chromatograms of the tars collected after reaction in comparison with the corresponding fresh tar fractions: presence of excluded peaks and the lift-off of the retained bands as well as the maximum intensity peaks appearing at shorter retention times (larger molecular size). This indicates that, as a result of interacting with the anode powders, both Fraction 1 and Fraction 2 evolved towards a material with heavier molecular weight distribution. Although a shift of the molecular weight distributions towards heavier species could also be

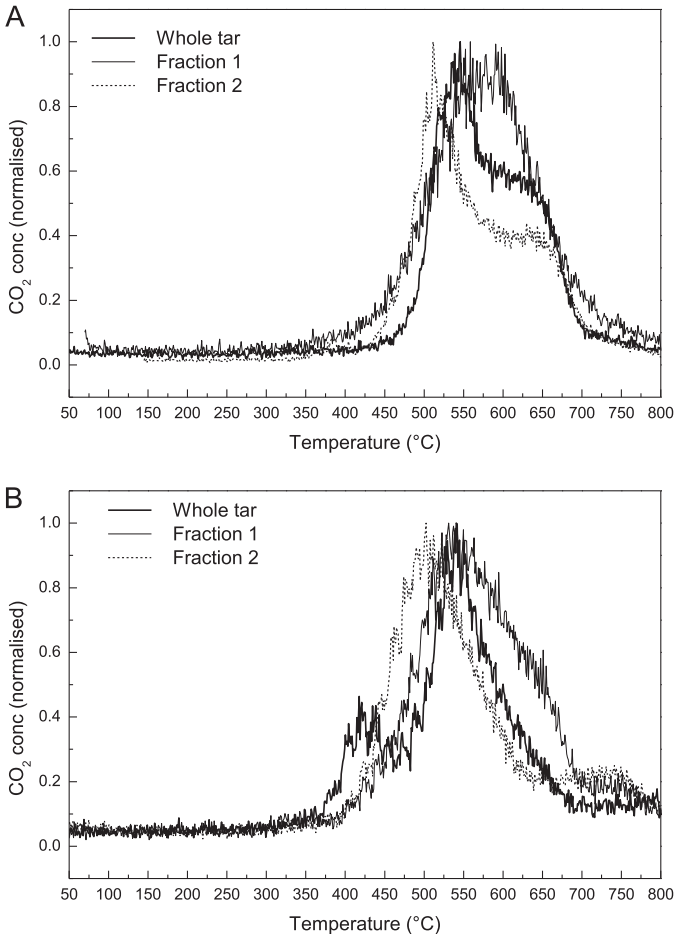

Fig. 6. Temperature programmed oxidation (TPO) curves of solids after the carbon deposition tests with A) Ni/YSZ and B) Ni/CGO.

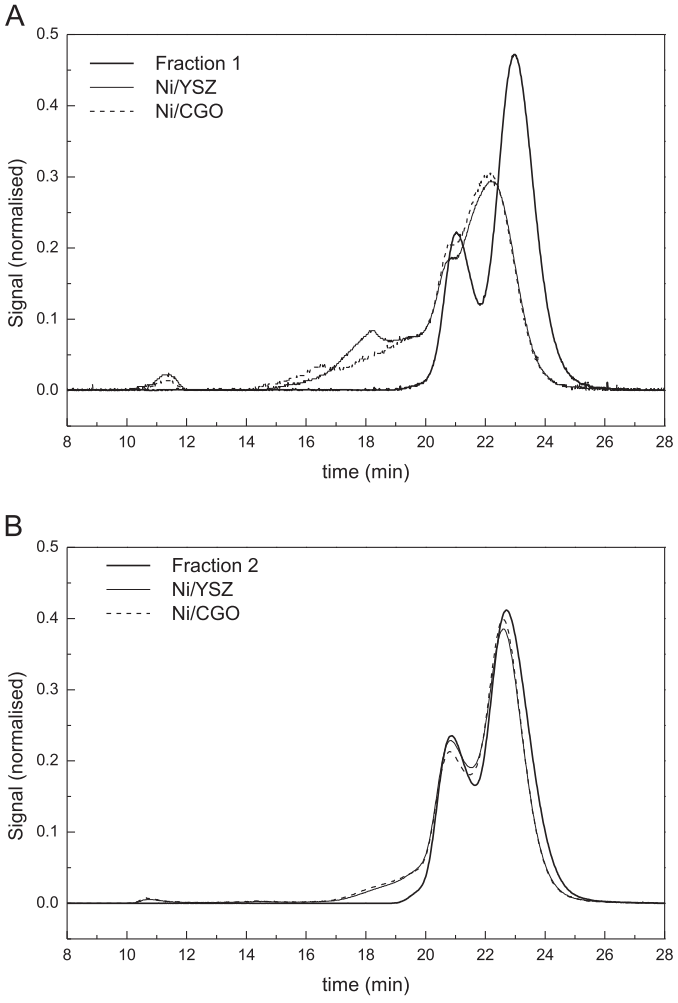

Fig. 7. SEC chromatograms of the condensable tar samples recovered after the carbon deposition tests with A) Fraction 1 and B) Fraction 2.

observed if light ends were removed during the tar recovery process, it is clear from these chromatograms that the distributions extended to high molecular weights well beyond the range present in the original fraction, indicating the occurrence of condensation or polymerization reactions. This fact is especially evident in the case of Fraction 1, which showed a lift-off at masses around 60,000 u, as compared with 1000 u for the fresh sample. Likewise, the maximum intensity peak in the chromatograms of the tars collected downstream from the bed was located at 180 u, while this peak appeared at 120 u in the chromatogram of the fresh tar.

The synchronous UV-F spectra of the tar samples recovered after each experiment are plotted in Fig. 8A and B, for the series of tests with Fraction 1 and Fraction 2, respectively. The spectrum of the corresponding fresh tar fraction is also presented, to allow comparison. Fig. 8A shows that the spectra of the recovered tars from Fraction 1 experiments appeared at longer wavelengths than the fresh tar. On the other hand, Fraction 2 (Fig. 8B) showed much narrower differences between the range of chromophore groups detected after and before the runs, although there was also in this case a shift towards longer wavelengths after the runs. These shifts in the spectra indicate the presence of larger aromatic chromophore sizes in the samples of tars exposed to anode materials. Again, the presence of these larger aromatic groups can be explained by condensation reactions undergone by the tar.

Fig. 9 presents the GC chromatograms of the condensable tar samples recovered after the carbon deposition tests using both materials Ni/YSZ and Ni/CGO. The results showed the same trends

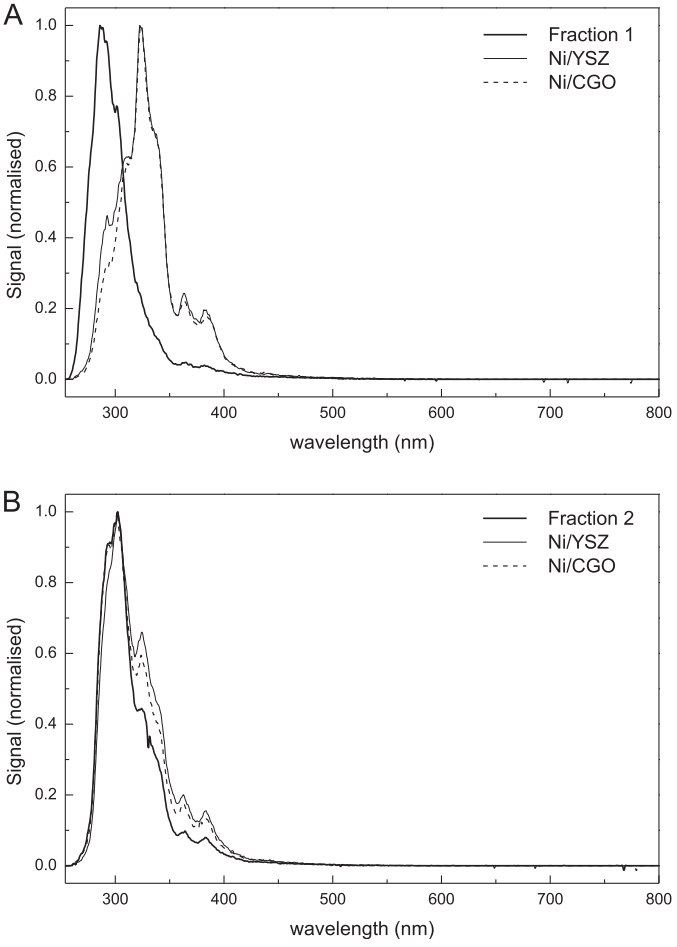

Fig. 8. UV-F synchronous spectra of the condensable tar samples recovered after the carbon deposition tests with A) Fraction 1 and B) Fraction 2.

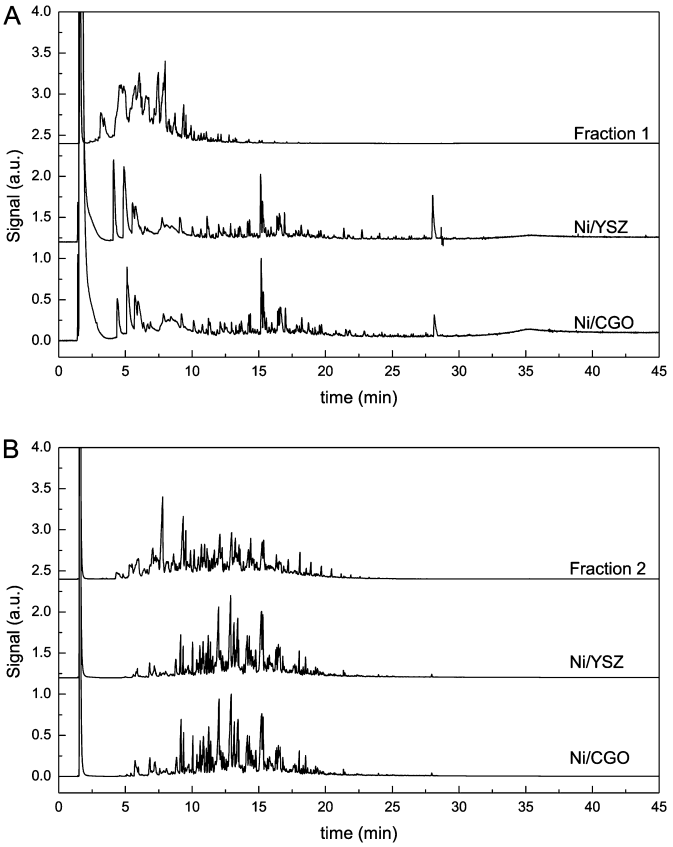

Fig. 9. GC chromatograms of the condensable tar samples recovered after the carbon deposition tests with A) Fraction 1 and B) Fraction 2.

as SEC, with a clear increase in molecular weight of the recovered tar in comparison with the original fractions. This trend was more evident for Fraction 1, with a clear reduction on the amount of compounds appearing from 5 to 10 min, and the detection of several compounds from 15 to 30 min that did not appear in the original chromatogram of Fraction 1. The results for Fraction 2 also showed an increase in the molecular weight distribution of the recovered tars, with a decrease in the light compounds range, and a higher concentration of the compounds in the range from 12 to 17 min. However, the upper limit in elution time did not increase respect to that of the original Fraction 2. These results show that the light ends of these fractions preferentially reacted on the anode material to form later-eluting compounds. It should be highlighted that the disappearance of light ends cannot be due to their evaporation during solvent drying after recovery. Firstly, this phenomenon was also observed in Fraction 2, which has higher boiling points than Fraction 1, for which compounds have been detected by GC. Secondly, new species were detected at longer elution times, which were not observed in the chromatograms of the original fractions.

In summary, tar analysis corroborated that lighter species are more reactive as lighter ends within each fraction reacted preferentially to form heavier hydrocarbons, containing larger polyaromatic groups, and carbon. The type of anode material (NiO/YSZ or NiO/CGO) had a minor effect of on the quality of tar obtained.

4. Conclusions

The effect of a gasification tar and its distillation fractions on the performance of two commercially available fuel cell anode

materials, Ni/YSZ (yttria stabilized zirconia) and Ni/CGO (gadolinium doped ceria), has been investigated in order to establish the relative contributions of different tar fractions to carbon formation on the anode.

The characterization of the tar and distillation fractions by ultimate analysis, SEC, UV-F and GC showed that each of the three fractions presented distinct features and differed from the whole tar.

Carbon formation was predominantly observed when the anodes were exposed to the lighter fractions (Fraction 1 and Fraction 2) as compared to the whole tar sample. Ni/CGO presented less degradation by carbon deposition than Ni/YSZ, with all the studied tar samples. TPO analyses revealed that the coke obtained from the medium-boiling point fraction (Fraction 2) was less graphitic than that formed on the anode after exposure to the lighter fraction (Fraction 1).

The characterization of the tars following contact with the anode materials suggests that both Fraction 1 and Fraction 2 became heavier due to reaction of their light ends in condensation/polymerization reactions on the anode. These changes were greater in Fraction 1 and the light end of Fraction 2. The picture emerging from this study shows that light fractions (and the light end within each fraction) are more reactive than heavy fractions and have a greater propensity to form larger polyaromatic species and eventually carbon on the anode surface. These tar light components are likely to adversely affect the operation of gasification-SOFC systems.

Acknowledgements

E.L. would like to acknowledge the Spanish Ministry of Education for financial support under postdoctoral grant (EX-2009-0015). The research leading to these results has received funding from the European Commission's Research Fund for Coal and Steel (RFCS) under grant agreement N° RFCS-CT-2010-00009.

References

[1] X. Zhang, S.H. Chan, G. Li, H.K. Ho, J. Li, Z. Feng, J. Power Sources 195 (2010) 685–702.
[2] T. Kivisaari, P. Björnbom, C. Sylwan, B. Jacquinot, D. Jansen, A. de Groot, Chem. Eng. J. 100 (2004) 167–180.
[3] A.O. Omosun, A. Bauen, N.P. Brandon, C.S. Adjiman, D. Hart, J. Power Sources 131 (2004) 96–106.
[4] K.D. Panopoulos, L.E. Fryda, J. Karl, S. Poulou, E. Kakaras, J. Power Sources 159 (2006) 570–585.
[5] J. Sadhukhan, Y. Zhao, N. Shah, N.P. Brandon, Chem. Eng. Sci. 65 (2010) 1942–1954.
[6] A. Abuadala, I. Dincer, Int. J. Hydrogen Energy 35 (2010) 13146–13157.
[7] J. Sadhukhan, Y. Zhao, M. Leach, N.P. Brandon, N. Shah, Ind. Eng. Chem. Res. 49 (2010) 11506–11516.
[8] R. Toonssen, N. Woudstra, A.H.M. Verkooijen, Int. J. Hydrogen Energy 35 (2010) 7594–7607.
[9] S. Shaffer, Fuel Cells Bull. 11 (2003) 2.
[10] R. Suwanwarangkul, E. Croiset, E. Entchev, S. Charojrochkul, M.D. Pritzker, M.W. Fowler, P.L. Douglas, S. Chewathanakup, H. Mahaudom, J. Power Sources 161 (2006) 308–322.
[11] Ph. Hofmann, A. Schweiger, L. Fryda, K.D. Panopoulos, U. Hohenwarter, J.D. Bentzen, J.P. Ouweltjes, J. Ahrenfeldt, U. Henriksen, E. Kakaras, J. Power Sources 173 (2007) 357–366.
[12] F.N. Cayan, M. Zhi, S.R. Pakalapati, I. Celik, N. Wu, R. Gemmen, J. Power Sources 185 (2008) 595–602.
[13] J. Bao, G.N. Krishnan, P. Jayaweera, J. Perez-Mariano, A. Sanjurjo, J. Power Sources 193 (2009) 607–616.
[14] J. Bao, G.N. Krishnan, P. Jayaweera, K.H. Lau, A. Sanjurjo, J. Power Sources 193 (2009) 617–624.
[15] J. Bao, G.N. Krishnan, P. Jayaweera, A. Sanjurjo, J. Power Sources 195 (2010) 1316–1324.
[16] A. Martinez, K. Gerdes, R. Gemmen, J. Poston, J. Power Sources 195 (2010) 5206–5212.
[17] C. Brage, Q. Yu, G. Chen, K. Sjöström, Biomass Bionergy 18 (2000) 87–91.
[18] Z. Abu-El-Rub, E.A. Bramer, G. Brem, Ind. Eng. Chem. Res. 43 (2004) 6911–6919.
[19] F. Pinto, H. Lopes, R. André, I. Gulyurtlu, I. Cabrita, Fuel 86 (2007) 2052–2063.
[20] L. Rabou, R. Zwart, B.J. Vreugdenhil, L. Bos, Energy Fuels 23 (2009) 6189–6198.
[21] A.G. Collot, Y. Zhuo, D.R. Dugwell, R. Kandiyoti, Fuel 78 (1999) 667–679.
[22] R. Kandiyoti, A.A. Herod, K.D. Bartle, Solid Fuels and Heavy Hydrocarbon Liquids: Thermal Characterization and Analysis, Elsevier, Amsterdam, 2006.
[23] A. Cousins, Y. Zhuo, A. George, N. Paterson, D. Dugwell, R. Kandiyoti, Energy Fuels 22 (2008) 2491–2503.
[24] T. Damartzis, A. Zabaniotou, Renew. Sustain. Energy Rev. 15 (2011) 366–378.
[25] M.M. Yung, W.S. Jablonski, K.A. Magrini-Bair, Energy Fuels 23 (2009) 1874–1887.
[26] G.J. Saunders, K. Kendall, J. Power Sources 106 (2002) 258–263.
[27] J. Mermelstein, M. Millan, N. Brandon, J. Power Sources 195 (2010) 1657–1666.
[28] F. Dabai, N. Paterson, M. Millan, P. Fennell, R. Kandiyoti, Energy Fuels 24 (2010) 4560–4570.
[29] D. Singh, E. Hernandez-Pacheco, P.N. Hutton, N. Patel, M.D. Mann, J. Power Sources 142 (2005) 194–199.
[30] G.J. Offer, J. Mermelstein, E. Brightman, N.P. Brandon, J. Am. Ceram. Soc. 92 (2009) 763–780.
[31] J. Mermelstein, N.P. Brandon, M. Millan, Energy Fuels 23 (2009) 5042–5048.
[32] T. Namioka, T. Naruse, R. Yamane, Int. J. Hydrogen Energy 36 (2011) 5581–5588.
[33] J. Mermelstein, M. Millan, N.P. Brandon, Chem. Eng. Sci. 64 (2009) 492–500.
[34] P.V. Aravind, J.P. Ouweltjes, N. Woudstra, G. Rietveld, Electrochem. Solid-State Lett. 11 (2008) B24–B28.
[35] M. Hauth, W. Lerch, K. König, J. Karl, J. Power Sources 196 (2011) 7144–7151.
[36] E. Lorente, M. Millan, N.P. Brandon, Int. J. Hydrogen Energy 37 (2012) 7271–7278.
[37] K. Nikooyeh, R. Clemmer, V. Alzate-Restrepo, J. Hill, Appl. Catal. A Gen. 347 (11) (2008) 106–111.
[38] C.M. Finnerty, N.J. Coe, R.H. Cunningham, R.M. Ormerod, Catal. Today 46 (1–2) (1998) 137–145.
[39] R.T. Baker, I.S. Metcalfe, Ind. Eng. Chem. Res. 34 (5) (1995) 1558–1565.
[40] F. Karaca, C.A. Islas, M. Millan, M. Behrouzi, T.J. Morgan, A.A. Herod, R. Kandiyoti, Energy Fuels 18 (2004) 778–788.
[41] C. Berrueco, S. Venditti, T.J. Morgan, P. Alvarez, M. Millan, A.A. Herod, R. Kandiyoti, Energy Fuels 22 (2008) 3265–3274.
[42] C.Z. Li, F. Wu, H.Y. Cai, R. Kandiyoti, Energy Fuels 8 (1994) 1039–1048.
[43] W.Z. Zhu, S.C. Deevi, Mater. Sci. Eng. 362 (2003) 228–239.
[44] I.C. Lewis, IC, Carbon 20 (1982), pp. 519–529.